

Article

Design of BiOCl/WO₃@Polyaniline Organic–Inorganic Nanocomposite Photocatalyst for the Efficient Decontamination of 2-Chlorophenol from Wastewater

Rajeev Kumar , Md. Abu Taleb , Mohamed A. Barakat *  and Bandar Al-Mur 

Department of Environmental Sciences, Faculty of Meteorology, Environment and Arid Land Agriculture, King Abdulaziz University, Jeddah 21589, Saudi Arabia

* Correspondence: mababdullah1@kau.edu.sa

Abstract: Advanced photocatalysts that can utilize solar energy for water purification applications are always needed. The present article reports a facile fabrication of tungsten oxide (WO₃)/bismuth oxychloride (BiOCl) immobilized on polyaniline (PAn) (BiOCl/WO₃@PAn) heterojunction nanocomposite photocatalyst. The designed nanocatalyst was tested for 2-chlorophenol (2-CP) decontamination from the aquatic system. Synthesized WO₃, BiOCl, and BiOCl/WO₃@PAn nanocomposites were distinguished via UV-DSR, photoluminescence, SEM, TEM, XRD, and XPS analysis. The combination of PAn with WO₃ and BiOCl showed a synergistic impact on the photocatalytic efficiency of the BiOCl/WO₃@PAn nanocomposite. The synthesized BiOCl/WO₃@PAn nanocomposite showed higher visible light absorption behavior and bandgap energy reduction than the WO₃ and BiOCl. The obtained data shows that 2-CP photocatalysis by the BiOCl/WO₃@PAn is controlled by degradation time, pH, and pollutant amount in the solution. The highest photocatalytic degradation of 2-CP (99.7%) was recorded at pH 5 and 25 mg/L concentration within 240 min. The photocatalysis mechanism and active radical scavenging study discovered that •O₂[−] and •OH, were responsible for the 2-CP mineralization onto the BiOCl/WO₃@PAn nanocomposite. The BiOCl/WO₃@PAn nanocomposite showed enhanced decontamination properties over pristine catalysts. The reusability of the synthesized BiOCl/WO₃@PAn nanocomposite was evaluated. It found that the photocatalyst could be recycled for up to four cycles for 2-CP degradation without significantly losing the photocatalytic properties. The fabricated BiOCl/WO₃@PAn nanocomposite catalyst presented exceptional catalytic and recycling properties, indicating an effective method for scavenging hazardous organic contaminants under solar irradiation and green technology for wastewater purification.

Keywords: photocatalysis; 2-chlorophenol; BiOCl/WO₃@PAn nanocomposite; wastewater purification



Citation: Kumar, R.; Taleb, M.A.; Barakat, M.A.; Al-Mur, B. Design of BiOCl/WO₃@Polyaniline Organic–Inorganic Nanocomposite Photocatalyst for the Efficient Decontamination of 2-Chlorophenol from Wastewater. *Catalysts* **2023**, *13*, 175. <https://doi.org/10.3390/catal13010175>

Academic Editors: Sheng Guo, Yazi Liu and Jun Li

Received: 15 December 2022

Revised: 1 January 2023

Accepted: 9 January 2023

Published: 11 January 2023



Copyright: © 2023 by the authors. Licensee MDPI, Basel, Switzerland. This article is an open access article distributed under the terms and conditions of the Creative Commons Attribution (CC BY) license (<https://creativecommons.org/licenses/by/4.0/>).

1. Introduction

Globally, natural water resources are facing contamination problems due to the mixing of unwanted substances [1,2]. Urbanization, industrialization, and anthropogenic activities such as releasing solvents, drugs, radioactive materials, and industrial wastes are directly or indirectly responsible for increasing water pollutants [3,4]. The wastewater from manufacturing, petroleum refineries, and textile industries is primarily accountable for hazardous organic pollutants, including dyes, phenol, and their derivatives [5–7]. The 2-chlorophenol is generated from oil refinery industries, and it is hazardous from 1 mg/L, thus having harmful effects on the living organism in the aquatic environment [8]. Therefore, reducing the concentration of 2-CP is needed to remove wastewater by applying appropriate methods.

Different treatment methods, including catalytic oxidation, adsorption, liquid–liquid extraction, thermal oxidation, distillation, membrane separation, photocatalysis, etc., have been used to scavenge 2-chlorophenol from wastewater [9–12]. An appropriate treatment

method selection depends on potential techniques' operating cost and removal efficiency. Photocatalytic oxidations have gained the great attention of scientists due to their removal efficiency of organic pollutants and the capacity of water, mineral ions, and carbon dioxide production as the product [13,14]. Therefore, researchers are using this method for water treatment and hydrogen production. Among other processes, photocatalysis using semiconductor materials is considered an efficient and advanced photochemical oxidation method for scavenging organic pollutants due to chemical stability, low cost, and capacity for complete mineralization. [15–17].

Semiconductor photocatalysis is one of the advanced photooxidation processes in which hydroxyl radicals are produced without using chemical reagents [18]. The hydroxyl radical with 2.8 V as a high oxidation potential can sharply trigger contaminants in wastewater for complete removal. In addition, semiconductors are promising photocatalysts because of their narrow bandgap energy (E_{bg}) among conduction and valence bands (CB and VB). To enhance the utilization capacity of visible light, the energy bandgap of potential catalysts and visible light should be within the range of 3.0 eV [19]. Researchers are using numerous semiconductor photocatalysts, including titanium oxide (TiO₂), copper (II) oxide (CuO), bismuth oxychloride (BiOCl), tungsten oxide (WO₃), etc. [20–22].

Among other semiconductor photocatalysts, WO₃ has a narrow bandgap (E_b 1.5–2.8 eV) and is a potential candidate for photocatalysis due to its exciting properties, including chemical, electrochemical, and optical features [23]. Compared to the other catalysts, tungsten oxide showed excellent chemical stability in triggering solar irradiation, promising photocorrosion resistance, and absorbing a wide range of visible spectrums [24]. On the other hand, a layered photocatalyst, bismuth oxychloride (BiOCl), has been explored as an eco-friendly candidate for environmental remediation because of its open crystal structure, nontoxicity, indirect-transition band, and excellent chemical stability and corrosion resistance [25]. Some researchers reported that semiconductor photocatalysts had shown some disadvantages, including swift recombination of electron–hole pairs, thus losing their photocatalytic performance, even though these are considered superior photocatalysts for the degradation of organic pollutants [26]. Therefore, to overcome such weaknesses of conventional semiconductor photocatalysts, scientists are trying to introduce novel composite photocatalysts using different catalysts, including polymer-like polyaniline (PAN). In polymeric semiconductors, the polyaniline showed excellent optoelectronic and photo-physical properties, including stability in excited states, tunable bandgap, extended surface area, thermal stability, chemical inertness, and high absorption area, etc. The presence of σ and π bond electronic cloud system in PAN shows a lower bandgap energy of 1.5 to 2.8 eV, and under light irradiation, it can act as an effective photosensitizer [14,27]. A literature review demonstrated that few articles had been published on synthesizing the binary composite of polyaniline/WO₃ and polyaniline/BiOCl in sensing, catalysis, and electrochromic applications [28,29]. Based on previous studies, a ternary composite of WO₃, BiOCl, and polyaniline could be an excellent semiconductor photocatalyst for decomposing toxic chemicals in wastewater under natural solar light.

This study aimed to prepare a bismuth oxychloride/tungsten oxide@polyaniline (BiOCl/WO₃@PAN) nanocomposite for the degradation of 2-CP from wastewater under solar light irradiation. The synthesized photocatalysts WO₃, BiOCl, and BiOCl/WO₃@Pan nanocomposite were characterized using scanning electron microscopy (SEM), X-ray diffraction (XRD), energy-dispersive X-ray spectroscopy (EDX) and photoluminescence spectroscopy (PL). Different operational factors, including the effect of solution pH, initial concentration, and reaction time, were evaluated for 2-CP photocatalytic degradation. The novelty of the BiOCl/WO₃@PAN nanocomposite is that integration of the semiconducting properties of the BiOCl, WO₃, and polyaniline and reduction of bandgap energy to enhance the photocatalytic properties in solar light.

2. Results and Discussion

2.1. Characterization of Photocatalysts

The surface morphology of synthesized photocatalysts, WO_3 , BiOCl , and $\text{BiOCl}/\text{WO}_3@PAn$ nanocomposite are depicted in Figure 1. The agglomerated irregular shape particle cluster of WO_3 can be seen in Figure 1a. Similar morphology of WO_3 is reported in earlier studies [30]. The SEM image of the BiOCl (Figure 1b) demonstrates the sheet-like morphology with different shapes and sizes. The morphology of the $\text{BiOCl}/\text{WO}_3@PAn$ nanocomposite is depicted in Figure 1c, which shows the well-distributed BiOCl covered with $\text{WO}_3@Pan$, indicating successful fabrication of $\text{BiOCl}/\text{WO}_3@PAn$ nanocomposite.

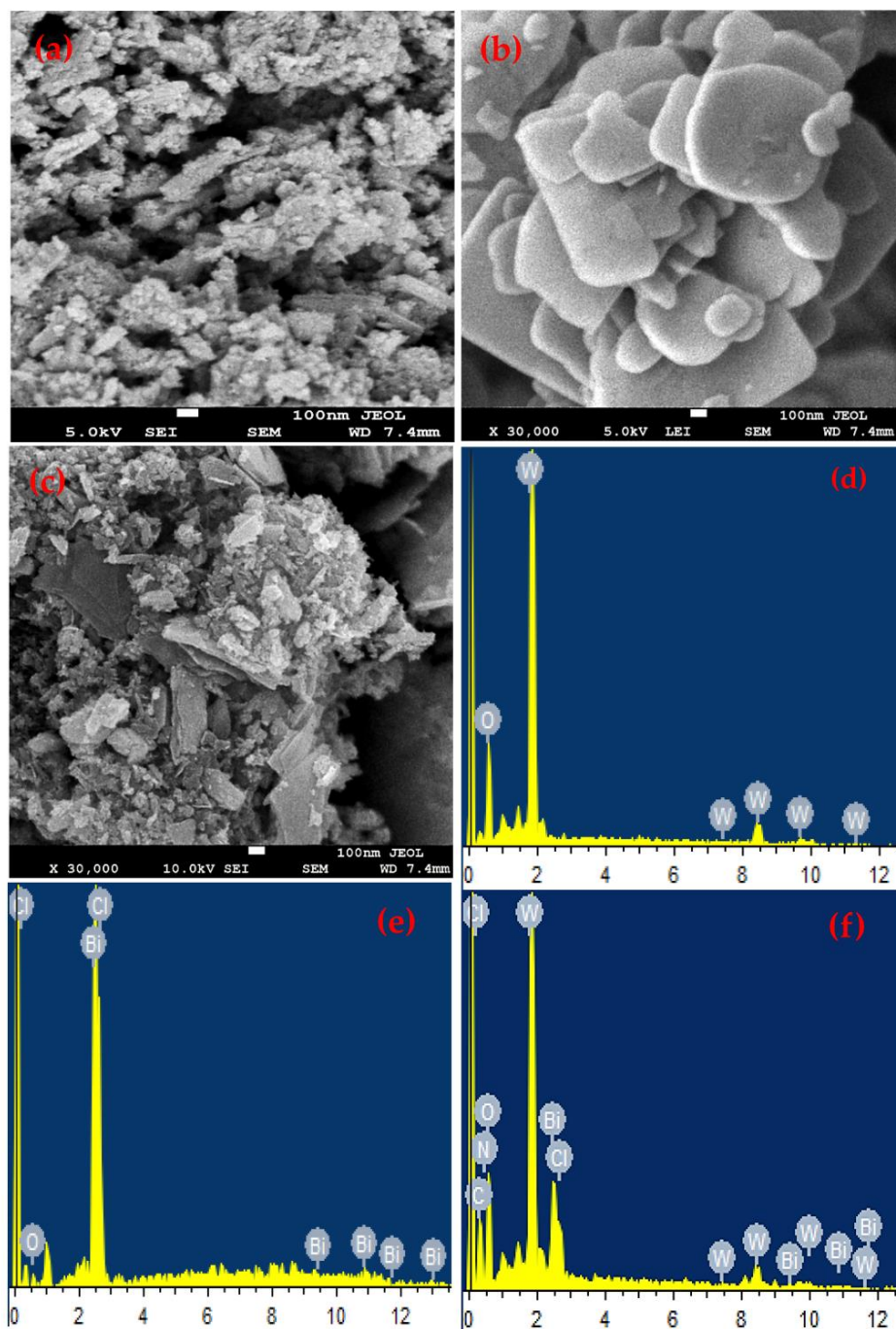


Figure 1. SEM images of (a) WO_3 (b) BiOCl (c) $\text{BiOCl}/\text{WO}_3@PAn$ nanocomposite and EDX analysis of (d) WO_3 , (e) BiOCl and, (f) $\text{BiOCl}/\text{WO}_3@PAn$ nanocomposite.

The elemental fractions of fabricated photocatalysts are also shown in Figure 1d–f. Compositions of chemical elements in the WO_3 , BiOCl, and BiOCl/ WO_3 @PAn nanocomposite were analyzed using energy-dispersive X-ray spectroscopy (EDX). The EDX analysis of WO_3 (Figure 2d) confirmed the existence of O and W with respective fractions of 77.94% and 22.06% (atomic %). The chemical elements in BiOCl are O (25.15%), Cl (22.35%), and Bi (52.50%) (Figure 2e). The elements observed in BiOCl/ WO_3 @PAn nanocomposite Figure 2f showed the existence of C, N, O, Cl, W and Bi with fractions of 43.9%, 1.8%, 38.2%, 3.61%, 8.85%, and 3.31%, respectively, which assured the successful fabrication of BiOCl/ WO_3 @PAn nanocomposite.

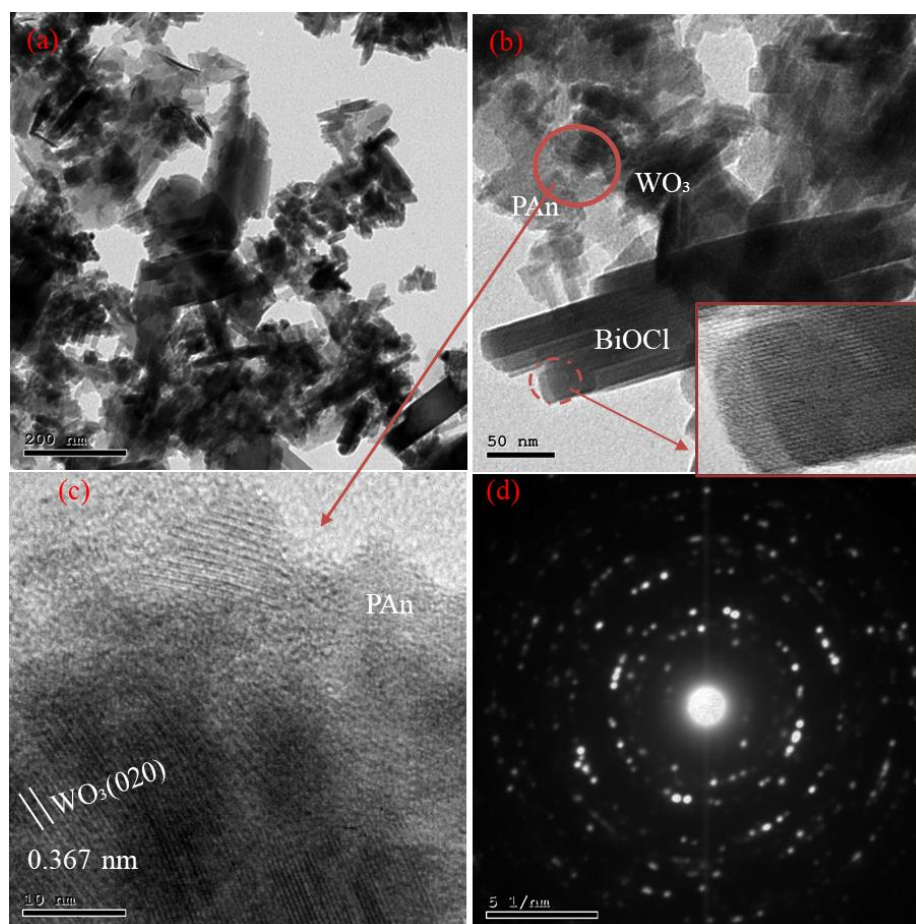


Figure 2. (a,b) TEM images, (c) HR-TEM image, and (d) SEAD pattern of BiOCl/ WO_3 @PAn nanocomposite.

The interaction and interfaces between the BiOCl, WO_3 , and PAn in BiOCl/ WO_3 @PAn nanocomposite were further observed using the TEM. The TEM images of the BiOCl/ WO_3 @PAn nanocomposite are shown in Figure 2. The distribution of the BiOCl, WO_3 , and PAn in BiOCl/ WO_3 @PAn nanocomposite can be seen in Figure 2a, showing some sheet-like structure surrounded by the WO_3 and PAn particles. Figure 2b shows the better morphology of the BiOCl/ WO_3 @PAn nanocomposite, demonstrating the good interactions between large BiOCl nanosheets and elongated WO_3 particles and PAn particles well matching with the SEM results. The HR-TEM images in Figure 2c show the lattice fringes of (020) planes belonging to WO_3 surrounded by a noncrystalline PAn matrix. The SEAD pattern of the BiOCl/ WO_3 @PAn nanocomposite shows the polycrystalline nature of the synthesized catalyst.

The phase structure of the fabricated photocatalysts WO_3 , BiOCl, and BiOCl/ WO_3 @PAn nanocomposite were analyzed using X-ray powder diffraction (XRD). The obtained spectrum is illustrated in Figure 3. The XRD pattern of WO_3 reflected peaks at $2\theta^\circ$ indexed

panels are 14.08 (100), 23.03 (001), 24.19 (020), 27.02 (101), 28.08 (200), 36.64 (201), 50.08 (220), 55.80 (221), 58.12 (400) and 63.33 (401) those are matching with the JCPDS-card number 00-035-1001 in the form of tungsten oxide hydrate. The XRD pattern of BiOCl showing the peaks at corresponding $2\theta^\circ$ planes is 11.98 (001), 24.16 (002), 25.82 (101), 32.51 (110), 33.41 (102), 40.86 (112), 46.64 (200), 48.40 (201), 49.61 (113), 52.43 (202), 54.05 (211), 58.62 (212), 60.66 (114), 75.16 (301) and 77.67 (310) those are in the form of bismoclite, bismuth oxide chloride matching with JCPDS card number-00-003-1126, 00-006-0249, 00-003-1125, respectively [31]. The obtained peaks for BiOCl/WO₃@PAn nanocomposite illustrated in Figure 2 detected at $2\theta^\circ$ are 11.98 (001), 22.95 (001), 24.19 (020), 25.86 (101), 27.7 (120), 32.51 (110), 33.55 (102), 36.63 (030), 44.44 (230), 46.63 (200), 49.76 (040), 54.16 (211) and 55.79 (041) belongs to the BiOCl and WO₃ in the BiOCl/WO₃@PAn nanocomposite. The XRD pattern of WO₃/BiOCl/PAn nanocomposite showed similar reflection peaks as observed for tungsten oxide, bismoclite, and bismuth oxide chloride, with a little shift in the peak position and intensity. The peak for the polyaniline was not observed due to its amorphous nature and small amount [2].

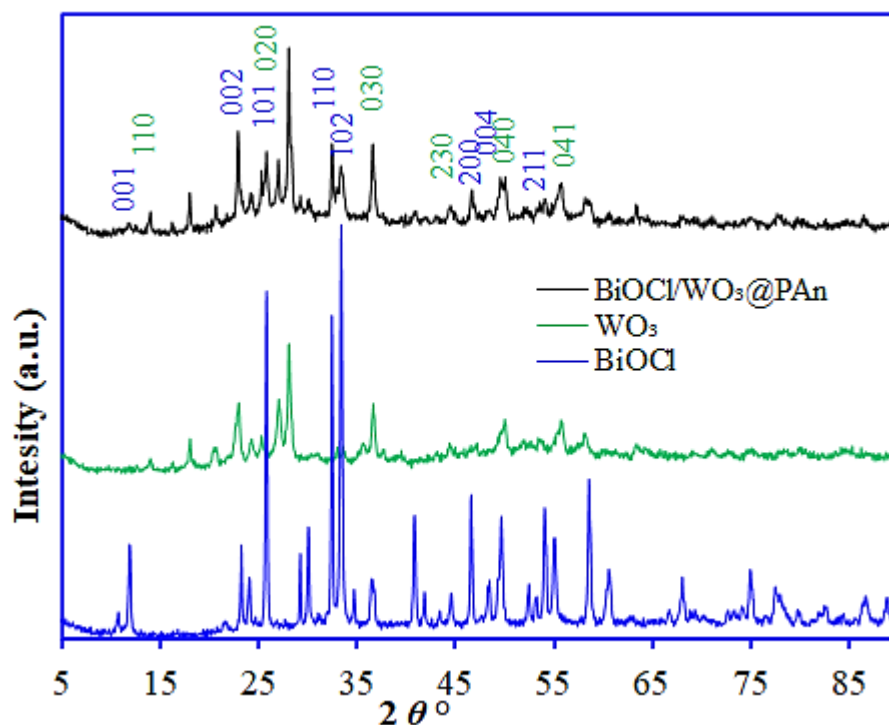


Figure 3. XRD patterns of BiOCl, WO₃, and BiOCl/WO₃@PAn nanocomposite.

The XPS analysis of BiOCl/WO₃@PAn nanocomposite, presented in Figure 4, exhibited the existence of C1s, O1s, W4f, N1s, Bi4f, Cl2p, etc., with the corresponding peaks and the percentage of chemical elements—carbon (49.7%), oxygen (32.3%), tungsten (7.8%), nitrogen (5.8%), bismuth (3.3%), and chlorine (1.1%)—as depicted in the wide survey scan in Figure 4a. The C1s spectra can be deconvoluted into 284.59, 285.84, and 288.95 eV peaks, as illustrated in Figure 4b. The O1s spectra contain two corresponding peaks at 530.91 and 532.21 eV, as depicted in Figure 4c. On the other hand, two peaks at 34.05 and 36.14 eV were recorded for W4f, as presented in Figure 4d. In addition, the other two peaks were deconvoluted into 401.88 and 403.91 eV for N1s spectra, as illustrated in Figure 4e. The Bi 4f spectrum is exhibited in Figure 4f with corresponding four spectra at 158.90, 159.89, 164.22, and 165.09 eV [32]. The Cl2p spectra were shown in Figure 4g of three peaks at 198.54, 200.01, and 201.61 eV. The chemical elements of C, O, N, W, Bi, and Cl, with their corresponding peaks and spectrum, confirm the successful fabrication of BiOCl/WO₃@PAn nanocomposite [33].

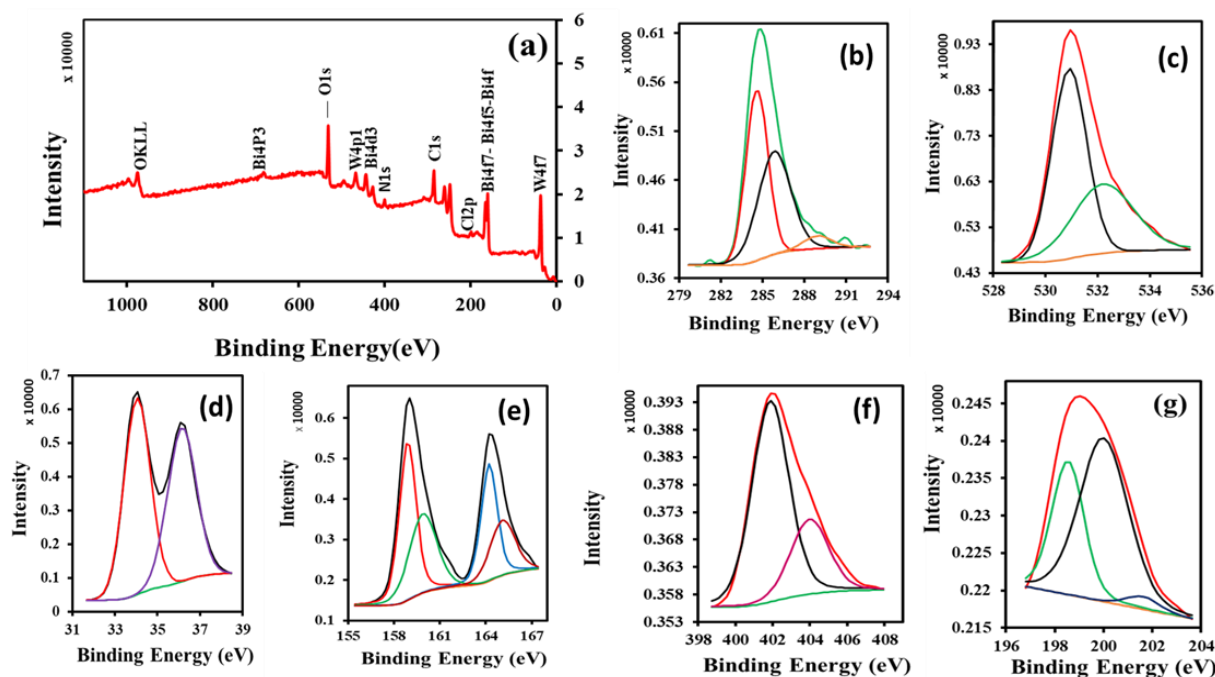


Figure 4. XPS spectra of BiOCl/WO₃@PAN nanocomposite, survey scan (a), C1s (b) O1s (c), W4f (d), N1s (e), Bi4f (f), Cl2p (g).

The light absorption properties of the BiOCl, WO₃, and BiOCl/WO₃@PAN nanocomposite were observed using UV-visible absorbance and photoluminescence spectroscopy. The UV-visible absorption spectra of the BiOCl, WO₃, and BiOCl/WO₃@PAN nanocomposite are depicted in Figure 5a. The observed spectra reveal that BiOCl/WO₃@PAN nanocomposite showed the highest absorption of light in the visible region, while BiOCl and WO₃ showed absorption edges around 380 nm and 410 nm. The absorption peak edge for BiOCl/WO₃@PAN nanocomposite is around 580 nm, indicating that coupling of the BiOCl, WO₃, and PAN enhances the light absorption properties of the catalyst, which may favor the decomposition of the organic pollutants. A continuous increase in light absorption is mainly due to the polyaniline, which helps in the absorption of more photons from the solar spectrum, separates the produced electrons and holes, and generates more active radical species for the decomposition of the pollutant molecules [34]. The reduction in the bandgap energy of the BiOCl/WO₃@PAN nanocomposite compared to BiOCl and WO₃ indicates that the nanocomposite could be a more effective photocatalyst (Figure 5b,c). To confirm the reduction in the charge recombination, PL analysis of the BiOCl, WO₃, and BiOCl/WO₃@PAN nanocomposite was performed, and the results are demonstrated in Figure 5d. The PL spectrum indicated the highest intensity for BiOCl and lowest intensity for BiOCl/WO₃@PAN nanocomposite, suggesting a reduction in the recombination rate of the photogenerated species [35].

2.2. Photocatalytic Studies

Photocatalytic degradation of 2-CP was evaluated under sunlight illumination using 0.05 g of catalyst in 100 mL of 25 mg/L 2-CP concentration at pH-5 for 4 h reaction time. The adsorption was conducted for the initial 30 min to establish the equilibrium under the dark condition. Parallel photolysis of 2-CP (without catalysts) was also investigated under sunlight irradiation. The experimental results are displayed in Figure 6a, the 2-CP degradation using BiOCl, WO₃, and BiOCl/WO₃@PAN nanocomposite was significantly higher than the photolysis. About 99.58% 2-CP removal efficiency was attained by fabricated BiOCl/WO₃@PAN nanocomposite, which is much higher than the BiOCl, and WO₃. The BiOCl/WO₃@PAN photocatalyst shows high removal capacity due to enhanced visible light absorption properties and narrow bandgap energy than BiOCl, and WO₃ [33]. The bandgap

energy of the BiOCl, WO₃, and BiOCl/WO₃@PAn nanocomposite were observed from plot 5b as 3.42 eV, 2.9 eV, and 2.33 eV. The lower bandgap energy of the BiOCl/WO₃@PAn nanocomposite suppresses the recombination of the electron–hole pair and produces a large number of active radicals for the decomposition of the 2-CP molecules [36]. The interfacial contact between BiOCl, WO₃, and PAn considerably enhances the surface charge separation and plays a synergistic effect to enhance the photocatalytic property of the BiOCl/WO₃@PAn nanocomposite. Under solar light irradiation, photogenerated electrons moved from the valance band (VB) to the conduction band (CB) of the semiconductor photocatalyst and moved quickly to the CB of BiOCl and WO₃, thus successfully suppressing the recombination of the charged electrons and holes [33,36].

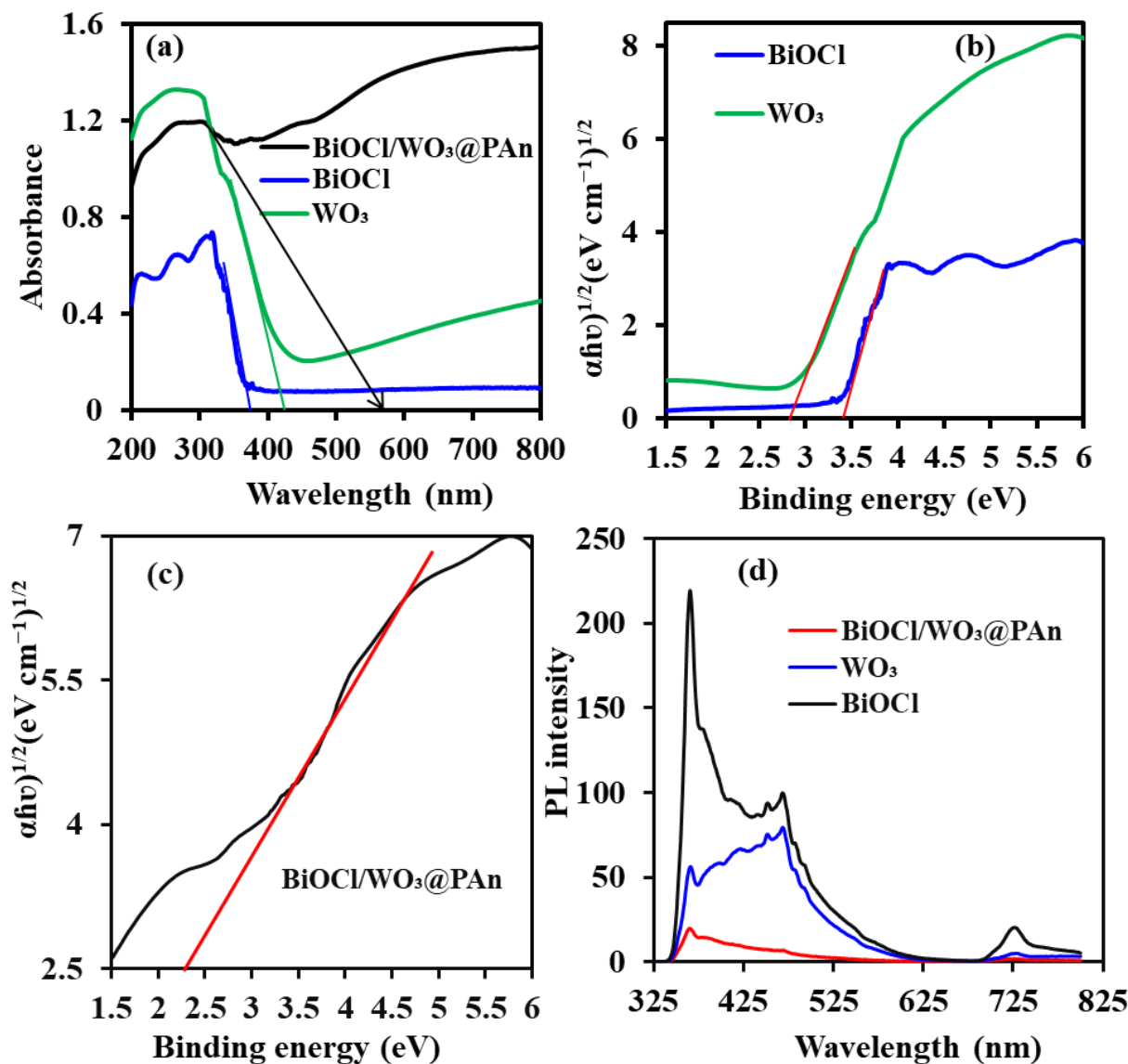


Figure 5. (a) UV-visible absorbance spectra, (b,c) plots for the bandgap energy analysis, and (d) photoluminescence spectra of the BiOCl, WO₃ and BiOCl/WO₃@PAn nanocomposite.

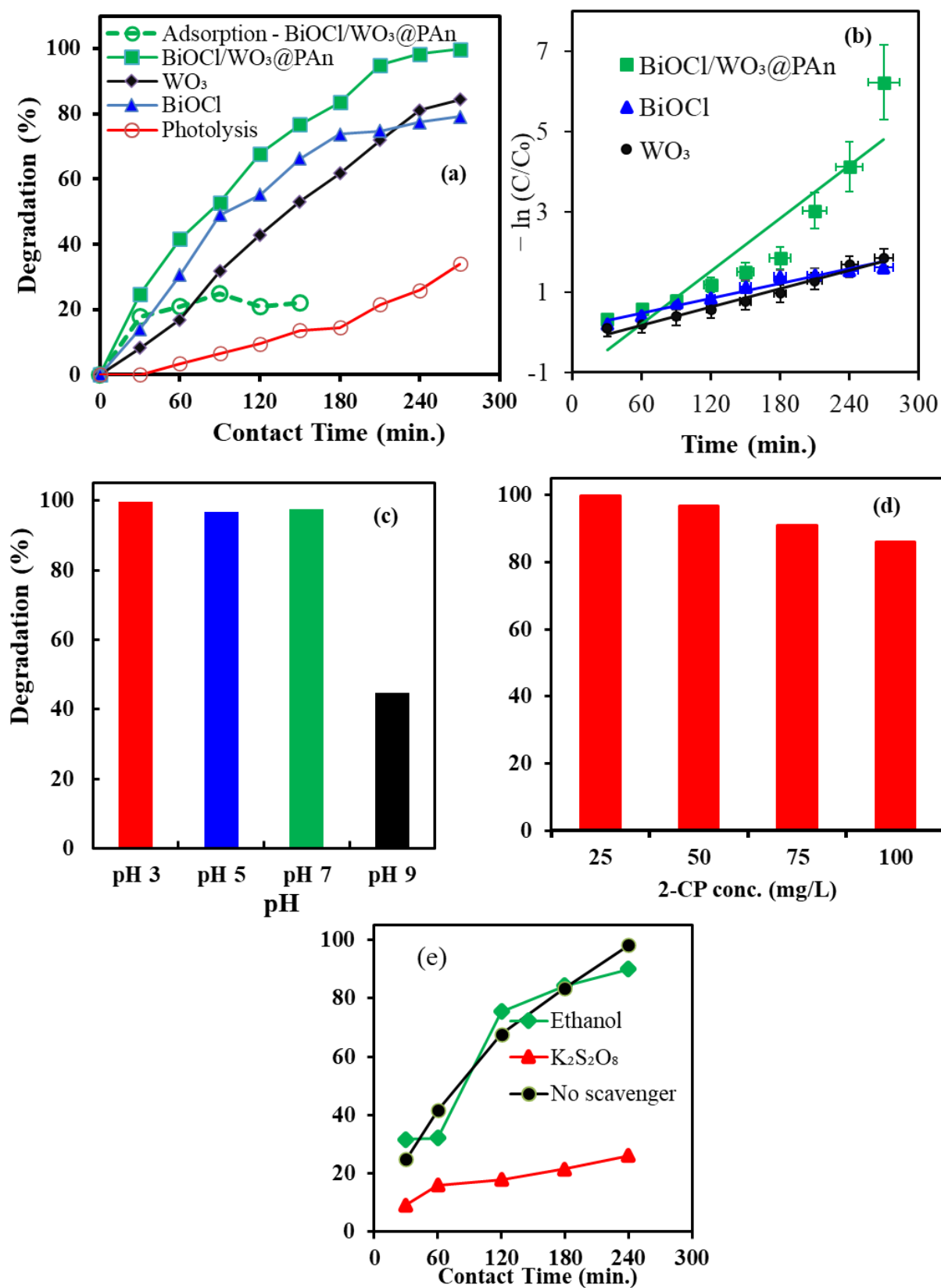


Figure 6. (a) Photocatalytic properties of BiOCl, WO₃ and BiOCl/WO₃@PAn for the decomposition of 2-CP under solar light irradiation. (b) Pseudo-first-order kinetic plot of 2-CP degradation. (c) Degradation of the 2-CP onto BiOCl/WO₃@PAn over a wide range of solution pH. (d) Effect of 2-CP concentration on the BiOCl/WO₃@PAn efficiency. (e) Photocatalytic degradation of 2-CP onto BiOCl/WO₃@PAn in the presence of active radical scavengers.

The photocatalytic degradation kinetics of 2-CP onto BiOCl, WO₃, and BiOCl/WO₃@PAn nanocomposite was investigated by fitting the kinetics data to the pseudo-first-order kinetic model:

$$-\ln(C/C_0) = k_{ap} t \quad (1)$$

where C₀ and C are the 2-CP concentration (mg/L) at initial and after time t. k_{ap} is the apparent rate constant. Figure 6b shows the kinetic plot of the 2-CP degradation. The rate constant k_{ap} values are 0.0061, 0.0076, and 0.021 min⁻¹ for BiOCl, WO₃, and BiOCl/WO₃@PAn nanocomposite. The most effective rate constant k_{ap} value was obtained for BiOCl/WO₃@PAn nanocomposite, indicating that synthesized nanocomposite is the most suitable catalyst for the degradation of 2-CP.

The solution pH is one of the vital parameters of photocatalysis. The pH influences the degradation of targeted pollutants due to photocatalyst interaction and surface charges [36]. The surface interactions between the BiOCl/WO₃@PAn nanocomposite and 2-CP molecules affect the degradation process under solar light illumination. To evaluate the effect the solution pH on 2-CP degradation onto BiOCl/WO₃@PAn nanocomposite, the photocatalytic activity was investigated at the pH value (3, 5, 7, 9) at an initial 2-CP concentration of 25 mg/L and 0.05 g of photocatalyst for a 100 mL sample. The experimental results in Figure 5c showing the maximum 2-CP degradation were recorded at pH 3–7. Thereafter, the degradation decreases with increases of pH value up to 9. The mechanism behind the higher decomposition at acidic and neutral pH can be interpreted based on the pK_a of 2-CP, which is ≈8.5. The 2-CP molecules exist as neutral species at the pH below pK_a values and do not show any repulsion with BiOCl/WO₃@PAn nanocomposite [37]. With the rise in the solution pH above 8.5, a negative charge is generated on 2-CP due to deprotonation, which showed the electrostatic repulsion with the BiOCl/WO₃@PAn nanocomposite [38]. Therefore, less decomposition was recorded due to the lack of interaction between 2-CP and BiOCl/WO₃@PAn nanocomposite.

The photocatalytic activity of BiOCl/WO₃@PAn nanocomposite was examined at different concentrations of 2-CP (25 to 100 mg/L). The experiment was conducted at pH 5 with 0.05 g BiOCl/WO₃@PAn mass in 100 mL of solution. The 2-CP degradation decreased with increases in concentration, as displayed in Figure 6d. The lower concentration (25 mg/L) of 2-CP was favorable for maximum degradation (99.7%), and degradation gradually decreased with increases in pollutant concentration. BiOCl/WO₃@PAn nanocomposite activity declined as higher pollutant concentration increased the viscosity and decreased optical density, which reduced the penetration of the photons into the solution, subsequently decreasing the photoexcitation of electrons [39].

To evaluate the effect of active radical scavengers on 2-CP degradation with the BiOCl/WO₃@PAn nanocomposite, an experiment was conducted in the presence of ethanol and potassium persulfate (K₂S₂O₈) at pH 5 and 25 mg/L of concentration and 0.05 g catalyst in a 100 mL sample [40]. The results illustrated in Figure 6e indicated that the 2-CP degradation dramatically decreased in the presence of K₂S₂O₈, as only 26% removal occurred while 99.7% degradation was attained without any scavengers. On the other hand, 90% of 2-CP degradation was recorded in the presence of ethanol, which was closer to the actual degradation of 2-CP using BiOCl/WO₃@PAn nanocomposite. K₂S₂O₈ is an •O₂⁻ scavenger (superoxide radical), and ethanol is an •OH scavenger (hydroxyl radical). The results demonstrated that photocatalytically produced superoxide radicals absorbed by the K₂S₂O₈ resulted in a noticeable reduction in the degradation process, while the presence of ethanol slightly decreased the photocatalysis of 2-CP. These results suggested that •O₂⁻ radicals are the main active species involved in decomposition process.

2.3. Reusability of BiOCl/WO₃@PAn Nanocomposite

The reusability of photocatalysts is one of the vital characteristics of commercial use. The reusability of BiOCl/WO₃@PAn nanocomposite was evaluated for 2-CP degradation under optimum conditions. The used BiOCl/WO₃@PAn nanocomposite was washed with deionized water and dried at 80 °C before reuse. Experimental results are shown in Figure 7,

indicating that BiOCl/WO₃@PAn nanocomposite is effective after fourfold reuse. The efficacy of the BiOCl/WO₃@PAn nanocomposite in 2-CP degradation negligibly decreased with the number of cycles. These results suggest that BiOCl/WO₃@PAn nanocomposite is stable and can be used several times.

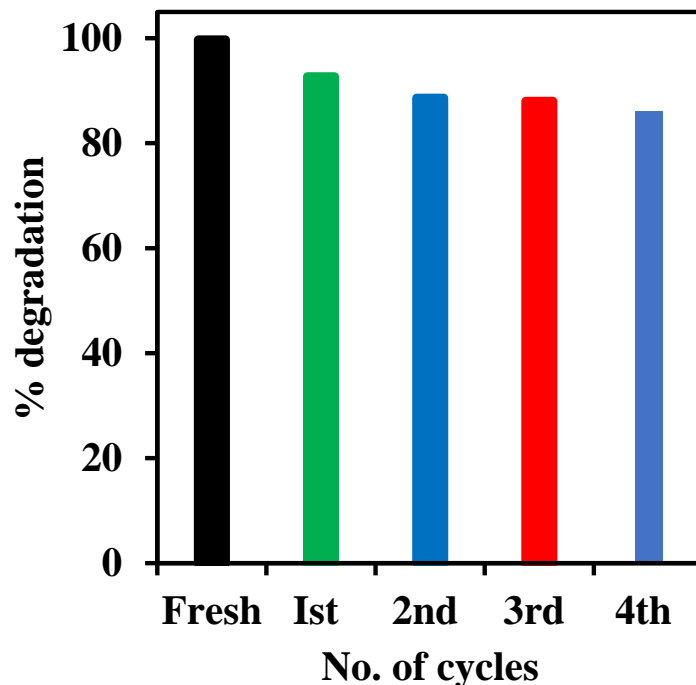
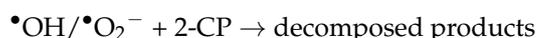
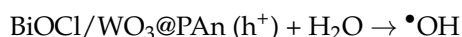
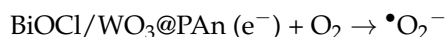


Figure 7. The reusability of BiOCl/WO₃@PAn nanocomposite for 2-CP degradation (conc. 25 mg/L, pH-5, catalyst mass 0.05 g, volume 100 mL, time 4 h.).

2.4. Photocatalysis Mechanism

The photocatalytic decomposition mechanism of the 2-CP onto BiOCl/WO₃@PAn nanocomposite is shown in Figure 8. The optical analysis results demonstrated that BiOCl/WO₃@PAn nanocomposite has the lowest bandgap energy (2.33 eV) compared to BiOCl (3.42 eV) and WO₃ (2.9 eV). Under solar light illumination, the photogenerated electrons and holes move according to the scheme presented in Figure 8. The photogenerated electrons from HOMO of PAn migrated to its LUMO [41]. These electrons further shifted to the conduction band of BiOCl. The electrons from CB of BiOCl transferred to the CB of WO₃. At the same time, h⁺ from VB of WO₃ went to VB of BiOCl and to HOMO of the PAn. The separation and transfer of the charge species are very fast and give the active radical species. The •O₂[−] are produced by the interaction of excited e[−] with O₂ on BiOCl/WO₃@PAn nanocomposite surface. Similarly, •OH radicals are produced by the h⁺ after the reaction with H₂O molecules [42,43]. A detailed reaction mechanism for the active radical generation is shown in the following equations.



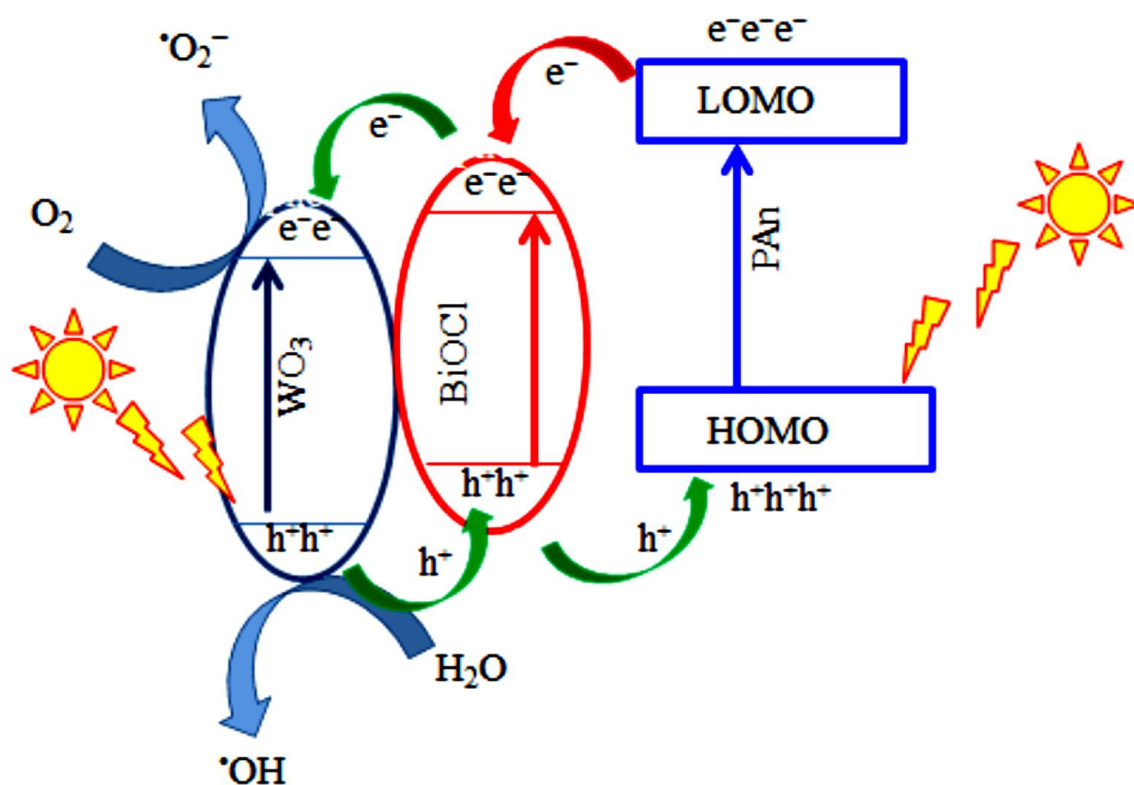


Figure 8. A proposed mechanism for the charge separation and generation of the active radical species on the surface of BiOCl/WO₃@PAn nanocomposite for 2-CP degradation.

2.5. Comparison of Photocatalytic Properties

The comparison of the photocatalytic properties of various photocatalysts with the BiOCl/WO₃@PAn nanocomposite for 2-CP decomposition is summarized in Table 1. Photocatalysis is highly dependent on experimental conditions. Therefore, a comparison of the photocatalytic properties of various photocatalysts and experimental conditions is included in Table 1. The results demonstrated that BiOCl/WO₃@PAn nanocomposite is highly efficient compared to previously reported photocatalysts.

Table 1. Comparison of the various catalysts' photocatalytic properties for 2-CP decomposition.

Photocatalysts/Materials	Photocatalytic Efficiency (%)	Conditions					Ref.
		Source of light	pH	Mass (g)	Time (min.)	Conc. (mg/L)	
NiO@Pani-MoS ₂ thin film	90	Solar light	7.0	0.03	60	25	[44]
Carbon nitride-titania nanotubes	70.25	Visible light	7.0	0.05	180	40	[45]
Carbon nitride-titania nanotubes	25.02	UV light	7.0	0.05	180	40	[45]
5% Ag-doped TiO ₂	74	UV light	10.5	0.005	150	50	[45]
0.2% Ru/TiO ₂	53	UV light	6.0	0.002	-	100	[46]
ZnO/Clay	88	Solar light	8.7	0.2	-	20	[47]
CuO-GO/TiO ₂	68	Visible light	5.0	0.5	180	100	[48]
Rb _{0.27} WO ₃	39	Visible light	7.0	0.05	210	80	[49]
NiFe-CLDH	45	Visible light	7.0	0.05	210	80	[49]
Carbon nanomaterials (CNMs)	79.64	Solar light	6.3	0.01	160	5	[50]
BiOCl/WO ₃ @PAn	99.7	Solar light	5	0.05	240	25	This study

3. Materials and Methods

3.1. Chemicals and Instrumentation

The polyaniline was prepared using the pure grade of aniline (Sigma-Aldrich Co., USA) and ammonium persulfate $(\text{NH}_4)_2\text{S}_2\text{O}_8$ (BHD Chemical, Poole, England). The other chemicals, such as sodium bismuthate (NaBiO_3) and sodium tungstate ($\text{Na}_2\text{WO}_4 \cdot 2\text{H}_2\text{O}$), were purchased as analytical grade (Sisco Research Laboratories Pvt. Ltd. India). The initial pH of 2-CP was adjusted by 1.0 M NaOH and/or HCl using a sensoin + PH3 m (Spain). Photocatalytic studies were performed under continuous stirring with a Scilogex LED magnetic digital stirrer under visible solar illumination. Surface morphology and texture of WO_3 , BiOCl, and BiOCl/ WO_3 @PAn nanocomposite were characterized by scanning electron microscopy using JSM-7500 F, JEOL, Japan. The crystal structure of photocatalysts was analyzed by X-ray powder diffraction (XRD) using a Rigaku Ultima IV, Tokyo, Japan. The chemical characterization and elemental analysis of materials were recorded using energy-dispersive X-ray spectroscopy (EDX). Photoluminescence spectra (PLS) of WO_3 , BiOCl, and BiOCl/ WO_3 @PAn nanocomposite were measured with an RF-5301PC Shimadzu, Kyoto, Japan, spectrofluorophotometer.

3.2. Synthesis of BiOCl/ WO_3 @PAn Nanocomposite

The polyaniline was prepared by adding 1.1 mL pure aniline in 40 mL of HCl (0.25 M) in an ice bath. An equimolar of ammonium persulfate prepared in 0.25 M HCl was mixed dropwise under continuous stirring for four hours. After some time, a blue-green precipitate of polyaniline was formed. A solution of sodium tungstate (0.9 g) and sodium bismuthate (0.4 g) prepared in 20 mL of 0.25 M HCl in a separated beaker was subsequently mixed with polyaniline solution under stirring for 40 min. Afterward, the material was heated at 120 °C for 30 min. Finally, the resultant photocatalyst was washed several times with deionized water and acetone, dried at 80 °C, and stored for photocatalytic studies. The dried mass of the BiOCl/ WO_3 @PAn nanocomposite was about 1.3 g, containing about 23.09% BiOCl, 34.61% WO_3 , and 42.30% PAN.

3.3. Photocatalytic Studies

Photodegradation studies were conducted with 0.05 g of photocatalysts in a 100 mL solution of 25 mg/L 2-CP concentration under natural sunlight illumination, continuous aeration, and shaking conditions. The dark adsorption experiments were also performed to find the equilibrium time by mixing 0.05 g of catalyst in 100 mL 2-CP solution of 25 mg/L concentration. The photolysis and photocatalysis of 2-CP degradation were investigated under continuous stirring and aeration conditions in solar light. The temperatures (31 ± 2 °C), humidity ($42 \pm 7\%$), and solar radiation intensity ($822 \times 10^2 \pm 92$ lux) were recorded during experiments. The consequences of solution pH on 2-CP photocatalytic degradation were evaluated in the pH range of 3–9 using 0.05 g catalyst in 100 mL of 2-CP solution (25 mg/L) under continuous aeration and shaking conditions for 240 min. The effect of contact times was considered to optimize the reaction time of photocatalytic degradation of 2-CP up to 240 min at pH 4.9 and 25 mg/L of 2-CP concentration. The effect of 2-CP concentration on its degradation onto BiOCl/ WO_3 @PAn nanocomposite was tested by varying the concentration between 25 to 100 mg/L at pH 4.9 for 240 min of solar light irradiation time. The decomposition of 2-CP in the presence of active radical scavengers was conducted by mixing the 0.05 mmol of ethanol and $\text{K}_2\text{S}_2\text{O}_8$ while 2-CP concentration was 25 mg/L, pH 4.9 and irradiation time was 240 min. The experimental samples were collected periodically and filtered using a 0.22 μm PTFE syringe membrane to avoid the remaining catalysts. The analysis of 2-CP was performed on a UV-visible DR 6000 spectrophotometer.

4. Conclusions

Herein, a BiOCl/ WO_3 @PAn nanocomposite photocatalyst was successfully fabricated. The synthesized photocatalyst was applied for degradation of 2-CP from wastewater under sunlight irradiation. The photocatalytic degradation of 2-CP onto BiOCl/ WO_3 @PAn

nanocomposite showed 99.7% at solution pH 5 and 25 mg/L concentration, which was significantly higher than the photolysis as well as pure WO_3 and BiOCl . Optical property analysis demonstrated incorporation of BiOCl and WO_3 with PAN enhanced the visible light absorption and suppressed the charged species' recombination rate. Active radical scavenging studies revealed that $\bullet\text{O}_2^-$ is the most active species in 2-CP decomposition. The composite photocatalyst was found to be a reusable catalyst for up to four successive regenerations for 2-CP photocatalysis under sunlight illumination. Therefore, $\text{BiOCl}/\text{WO}_3/\text{PAN}$ nanocomposite is considered a promising photocatalyst for degrading organic pollutants from wastewater.

Author Contributions: Conceptualization, methodology, and validation, R.K. and M.A.B.; formal analysis, M.A.T. and B.A.-M.; investigation, M.A.T.; resources, R.K., B.A.-M. and M.A.B.; data curation, M.A.T., writing—original draft preparation, R.K. and M.A.T.; writing—review and editing, B.A.-M. and M.A.B.; funding acquisition, R.K., M.A.B. and B.A.-M. All authors have read and agreed to the published version of the manuscript.

Funding: This project was funded by the Deanship of Scientific Research (DSR) at King Abdulaziz University, Jeddah (grant G: 250-155-1442).

Data Availability Statement: Available on request.

Acknowledgments: This project was funded by the Deanship of Scientific Research (DSR) at King Abdulaziz University, Jeddah (grant G: 250-155-1442). The authors, therefore, acknowledge with thanks the DSR for technical and financial support.

Conflicts of Interest: The authors declare no conflict of interest.

References

1. Isac, L.; Enesca, A. Recent Developments in ZnS-Based Nanostructures Photocatalysts for Wastewater Treatment. *Int. J. Mol. Sci.* **2022**, *23*, 15668. [[CrossRef](#)] [[PubMed](#)]
2. Bănăduc, D.; Simić, V.; Cianfaglione, K.; Barinova, S.; Afanasyev, S.; Öktener, A.; McCall, G.; Simić, S.; Curtean-Bănăduc, A. Freshwater as a Sustainable Resource and Generator of Secondary Resources in the 21st Century: Stressors, Threats, Risks, Management and Protection Strategies, and Conservation Approaches. *Int. J. Environ. Res. Public Health* **2022**, *19*, 16570. [[CrossRef](#)] [[PubMed](#)]
3. Isaacson, K.P.; Proctor, C.R.; Wang, Q.E.; Edwards, E.Y.; Noh, Y.; Shah, A.D.; Whelton, A.J. Drinking water contamination from the thermal degradation of plastics: Implications for wildfire and structure fire response. *Environ. Sci. Water Res. Technol.* **2021**, *7*, 274–284. [[CrossRef](#)]
4. Xu, Q.; Wu, B.; Chai, X. In Situ Remediation Technology for Heavy Metal Contaminated Sediment: A Review. *Int. J. Environ. Res. Public Health* **2022**, *19*, 16767. [[CrossRef](#)] [[PubMed](#)]
5. Yang, L.; Zhou, Q.; Zhang, H.; Zhang, X.; Xing, W.; Wang, Y.; Bai, P.; Yamauchi, M.; Chohji, T.; Zhang, L.; et al. Atmospheric Behaviour of Polycyclic and Nitro-Polycyclic Aromatic Hydrocarbons and Water-Soluble Inorganic Ions in Winter in Kirishima, a Typical Japanese Commercial City. *Int. J. Environ. Res. Public Health* **2021**, *18*, 688. [[CrossRef](#)] [[PubMed](#)]
6. Pham, T.H.; Jung, S.H.; Kim, Y.J.; Kim, T. Adsorptive removal and recovery of organic pollutants from wastewater using waste paper-derived carbon-based aerogel. *Chemosphere* **2021**, *268*, 129319. [[CrossRef](#)]
7. Adeniran, A.A.; Ayesu-Koranteng, E.; Shakantu, W. A Review of the Literature on the Environmental and Health Impact of Plastic Waste Pollutants in Sub-Saharan Africa. *Pollutants* **2022**, *2*, 531–545. [[CrossRef](#)]
8. Onkani, S.P.; Diagboya, P.N.; Mtunzi, F.M.; Klink, M.J.; Olu-Owolabi, B.I.; Pakade, V. Comparative study of the photocatalytic degradation of 2-chlorophenol under UV irradiation using pristine and Ag-doped species of TiO_2 , ZnO and ZnS photocatalysts. *J. Environ. Manag.* **2020**, *260*, 110145. [[CrossRef](#)] [[PubMed](#)]
9. Hadjltaief, H.B.; Sdiri, A.; Ltaief, W.; Da Costa, P.; Gálvez, M.E.; Ben Zina, M. Efficient removal of cadmium and 2-chlorophenol in aqueous systems by natural clay: Adsorption and photo-Fenton degradation processes. *Comptes Rendus Chim.* **2018**, *21*, 253–262. [[CrossRef](#)]
10. Qiu, J.; Liu, Q.; Qiu, Y.; Liu, F.; Wang, F. Enhanced Photocatalytic Degradation of P-Chlorophenol by ZnIn_2S_4 Nanoflowers Modified with Carbon Quantum Dots. *Catalysts* **2022**, *12*, 1545. [[CrossRef](#)]
11. Duan, J.; Ji, H.; Xu, T.; Pan, F.; Liu, X.; Liu, W.; Zhao, D. Simultaneous adsorption of uranium(VI) and 2-chlorophenol by activated carbon fiber supported/modified titanate nanotubes (TNTs/ACF): Effectiveness and synergistic effects. *Chem. Eng. J.* **2021**, *406*, 126752. [[CrossRef](#)]
12. Tan, J.; Wei, G.; Wang, Z.; Su, H.; Liu, L.; Li, C.; Bian, J. Application of $\text{Zn}_{1-x}\text{Cd}_x\text{S}$ Photocatalyst for Degradation of 2-CP and TC, Catalytic Mechanism. *Catalysts* **2022**, *12*, 1100. [[CrossRef](#)]

13. Siyal, A.A.; Shamsuddin, M.R.; Khahro, S.H.; Low, A.; Ayoub, M. Optimization of synthesis of geopolymer adsorbent for the effective removal of anionic surfactant from aqueous solution. *J. Environ. Chem. Eng.* **2021**, *9*, 104949. [[CrossRef](#)]
14. Ekande, O.S.; Kumar, M. Review on polyaniline as reductive photocatalyst for the construction of the visible light active heterojunction for the generation of reactive oxygen species. *J. Environ. Chem. Eng.* **2021**, *9*, 105725. [[CrossRef](#)]
15. Dharwadkar, S.; Yu, L.; Achari, G. Enhancement of LED based photocatalytic degradation of sulfolane by integration with oxidants and nanomaterials. *Chemosphere* **2021**, *263*, 128124. [[CrossRef](#)]
16. Pang, X.; Skillen, N.; Gunaratne, N.; Rooney, D.W.; Robertson, P.K. Removal of phthalates from aqueous solution by semiconductor photocatalysis: A review. *J. Hazard. Mater.* **2021**, *402*, 123461. [[CrossRef](#)]
17. Lei, Q.; Yang, S.; Ding, D.; Tan, J.; Liu, J.; Chen, R. Local-interaction-field-coupled semiconductor photocatalysis: Recent progress and future challenges. *J. Mater. Chem. A* **2021**, *9*, 2491–2525. [[CrossRef](#)]
18. Porcu, S.; Secci, F.; Ricci, P.C. Advances in Hybrid Composites for Photocatalytic Applications: A Review. *Molecules* **2022**, *27*, 6828. [[CrossRef](#)]
19. Kumar, R.; Abdel-Wahab, M.; Barakat, M.; Rashid, J.; Salah, N.; Al-Ghamdi, A.A. Role of N doping on the structural, optical and photocatalytic properties of the silver deposited ZnO thin films. *J. Taiwan Inst. Chem. Eng.* **2016**, *69*, 131–138. [[CrossRef](#)]
20. Gong, S.; Fan, J.; Cecen, V.; Huang, C.; Min, Y.; Xu, Q.; Li, H. Noble-metal and cocatalyst free W₂N/C/TiO₂ photocatalysts for efficient photocatalytic overall water splitting in visible and near-infrared light regions. *Chem. Eng. J.* **2021**, *405*, 126913. [[CrossRef](#)]
21. Rashid, J.; Karim, S.; Kumar, R.; Barakat, M.A.; Akram, B.; Hussain, N.; Bin, H.B.; Xu, M. A facile synthesis of bismuth oxychloride-graphene oxide composite for visible light photocatalysis of aqueous diclofenac sodium. *Sci. Rep.* **2020**, *10*, 14191. [[CrossRef](#)] [[PubMed](#)]
22. Ghattavi, S.; Nezamzadeh-Ejehieh, A. A double-Z-scheme ZnO/AgI/WO₃ photocatalyst with high visible light activity: Experimental design and mechanism pathway in the degradation of methylene blue. *J. Mol. Liq.* **2021**, *322*, 114563. [[CrossRef](#)]
23. Chu, S.; Hu, Y.; Zhang, J.; Cui, Z.; Shi, J.; Wang, Y.; Zou, Z. Constructing direct Z-scheme CuO/PI heterojunction for photocatalytic hydrogen evolution from water under solar driven. *Int. J. Hydrogen Energy* **2021**, *46*, 9064–9076. [[CrossRef](#)]
24. Yanyan, L.; Kurniawan, T.A.; Ying, Z.; Albadarin, A.B.; Walker, G. Enhanced photocatalytic degradation of acetaminophen from wastewater using WO₃/TiO₂/SiO₂ composite under UV–VIS irradiation. *J. Mol. Liq.* **2017**, *243*, 761–770. [[CrossRef](#)]
25. Mokhtarifar, M.; Nguyen, D.T.; Sakar, M.; Pedferri, M.; Asa, M.; Kaveh, R.; Diamanti, M.V.; Do, T.O. Mechanistic insights into photogenerated electrons store-and-charge in hydrogenated glucose template synthesized Pt: TiO₂/WO₃ photocatalyst for the round-the-clock decomposition of methanol. *Mater. Res. Bull.* **2021**, *4*, 111203. [[CrossRef](#)]
26. Wei, Z.; Li, W.; Hu, J.; Ma, X.; Zhu, Y. Interfacial internal electric field and oxygen vacancies synergistically enhance photocatalytic performance of bismuth oxychloride. *J. Hazard. Mater.* **2021**, *402*, 123470. [[CrossRef](#)] [[PubMed](#)]
27. Adhikari, S.P.; Dean, H.; Hood, Z.D.; Peng, R.; More, K.L.; Ivanov, I.; Wu, Z.; Lachgar, A. Visible-light-driven Bi₂O₃/WO₃ composites with enhanced photocatalytic activity. *RSC. Adv.* **2015**, *111*, 91094–91102. [[CrossRef](#)]
28. Scotland, K.M.; Strong, O.K.; Parnis, J.M.; Vreugdenhil, A.J. DFT modeling of polyaniline: A computational investigation into the structure and band gap of polyaniline. *Can. J. Chem.* **2022**, *100*, 162–167. [[CrossRef](#)]
29. He, W.; Zhao, Y.; Xiong, Y. Bilayer Polyaniline–WO₃ Thin-Film Sensors Sensitive to NO₂. *ACS Omega* **2020**, *5*, 9744–9751. [[CrossRef](#)]
30. Tang, Y.; Zhou, P.; Wang, K.; Lin, F.; Lai, J.; Chao, Y.; Li, H.; Guo, S. BiOCl/ultrathin polyaniline core/shell nanosheets with a sensitization mechanism for efficient visible-light-driven photocatalysis. *Sci. China Mater.* **2019**, *62*, 95–102. [[CrossRef](#)]
31. Wei, Y.-L.; Rong, B.; Chen, X.; Ding, Y.-Y.; Huang, Y.-F.; Fan, L.-Q.; Wu, J.-H. Porous and visible-light-driven p–n heterojunction constructed by Bi₂O₃ nanosheets and WO₃ microspheres with enhanced photocatalytic performance. *Sep. Purif. Technol.* **2021**, *256*, 117815. [[CrossRef](#)]
32. Yaghoubi-Berijani, M.; Bahramian, B. Preparation and measurement of properties of BiOBr/BiOCl/PANI ternary nanocomposite for highly efficient visible light photocatalytic applications. *Res. Chem. Intermed.* **2021**, *47*, 2311–2330. [[CrossRef](#)]
33. Huang, X.; Niu, Y.; Peng, Z.; Hu, W. Core–shell structured BiOCl@polydopamine hierarchical hollow microsphere for highly efficient photocatalysis. *Colloids Surfaces A: Physicochem. Eng. Asp.* **2019**, *580*, 123747. [[CrossRef](#)]
34. Mei, J.; Tao, Y.; Gao, C.; Zhu, Q.; Zhang, H.; Yu, J.; Fang, Z.; Xu, H.; Wang, Y.; Li, G. Photo-induced dye-sensitized BiPO₄/BiOCl system for stably treating persistent organic pollutants. *Appl. Catal. B Environ.* **2021**, *285*, 119841. [[CrossRef](#)]
35. Rahman, K.H.; Kar, A.K. Effect of band gap variation and sensitization process of polyaniline (PANI)-TiO₂ p–n heterojunction photocatalysts on the enhancement of photocatalytic degradation of toxic methylene blue with UV irradiation. *J. Environ. Chem. Eng.* **2020**, *8*, 104181. [[CrossRef](#)]
36. Xu, M.; Wang, Y.; Ha, E.; Zhang, H.; Li, C. Reduced graphene oxide/Bi₄O₅Br₂ nanocomposite with synergetic effects on improving adsorption and photocatalytic activity for the degradation of antibiotics. *Chemosphere* **2021**, *265*, 129013. [[CrossRef](#)]
37. Kanakaraju, D.; Ravichandar, S.; Lim, Y.C. Combined effects of adsorption and photocatalysis by hybrid TiO₂/ZnO-calcium alginate beads for the removal of copper. *Res. J. Environ. Sci.* **2017**, *55*, 214–223. [[CrossRef](#)]
38. Barakat, M.A.; Kumar, R.; Rashid, J.; Seliem, M.K.; Al-Mur, B.; El-Shishtawy, R.M. A novel CuO–Cu₂O/Ag–Ag₃PO₄ nanocomposite: Synthesis, characterization, and its application for 2-chlorophenol decontamination under visible light. *J. Taiwan Inst. Chem. Eng.* **2020**, *115*, 208–217. [[CrossRef](#)]
39. Anjum, M.; Oves, M.; Kumar, R.; Barakat, M.A. Fabrication of ZnO-ZnS@polyaniline nanohybrid for enhanced photocatalytic degradation of 2-chlorophenol and microbial contaminants in wastewater. *Int. Biodeter Biodeg.* **2017**, *119*, 66–77. [[CrossRef](#)]

40. Lin, Y.; Wu, S.; Yang, C.; Chen, M.; Li, X. Preparation of size-controlled silver phosphate catalysts and their enhanced photocatalysis performance via synergetic effect with MWCNTs and PANI. *Appl. Catal. B Environ.* **2019**, *245*, 71–86. [[CrossRef](#)]
41. Hou, J.; Jiang, T.; Wang, X.; Zhang, G.; Zou, J.J.; Cao, C. Variable dimensional structure and interface design of g-C₃N₄/BiOI composites with oxygen vacancy for improving visible-light photocatalytic properties. *J. Clean. Prod.* **2021**, *287*, 125072. [[CrossRef](#)]
42. Gilja, V.; Živković, I.; Klaser, T.; Skoko, Ž.; Kraljić Roković, M.; Hrnjak-Murčić, Z.; Žic, M. The Impact of In Situ Polymerization Conditions on the Structures and Properties of PANI/ZnO-Based Multiphase Composite Photocatalysts. *Catalysts* **2020**, *10*, 400. [[CrossRef](#)]
43. Bairamis, F.; Konstantinou, I. WO₃ Fibers/g-C₃N₄ Z-Scheme Heterostructure Photocatalysts for Simultaneous Oxidation/Reduction of Phenol/Cr (VI) in Aquatic Media. *Catalysts* **2021**, *11*, 792. [[CrossRef](#)]
44. Ansari, M.O.; Kumar, R.; Abdel-Wahab, M.; Taleb, A.; Barakat, M. Direct current deposited NiO on polyaniline@MoS₂ flexible thin film for highly efficient solar light mineralization of 2-chlorophenol: A mechanistic analysis. *J. Taiwan Inst. Chem. Eng.* **2021**, *129*, 370–380. [[CrossRef](#)]
45. Barakat, M.; Kumar, R.; O Eniola, J. Adsorption and photocatalytic scavenging of 2-chlorophenol using carbon nitride-titania nanotubes based nanocomposite: Experimental data, kinetics and mechanism. *Data Brief* **2021**, *34*, 106664. [[CrossRef](#)] [[PubMed](#)]
46. Elsalamony, R.A.; Mahmoud, S.A. Preparation of nanostructured ruthenium doped titania for the photocatalytic degradation of 2-chlorophenol under visible light. *Arab. J. Chem.* **2017**, *10*, 194–205. [[CrossRef](#)]
47. Zyoud, A.H.; Asaad, S.; Zyoud, S.H.; Zyoud, S.H.; Helal, M.H.; Qamhieh, N.; Hajamohideen, A.; Hilal, H.S. Raw clay supported ZnO nanoparticles in photodegradation of 2-chlorophenol under direct solar radiations. *J. Environ. Chem. Eng.* **2020**, *8*, 104227. [[CrossRef](#)]
48. Alafif, Z.O.; Anjum, M.; Kumar, R.; Abdelbasir, S.M.; Barakat, M.A. Synthesis of CuO–GO/TiO₂ visible light photocatalyst for 2-chlorophenol degradation, pretreatment of dairy wastewater and aerobic digestion. *Appl. Nanosci.* **2019**, *4*, 579–591. [[CrossRef](#)]
49. Zhao, G.; Zhang, D.; Huang, Y.; Yu, J.; Jiang, X.; Jiao, F. Highly efficient degradation of 2-chlorophenol and methylene blue with Rb_{0.27}WO₃/NiFe-CLDH composites under visible light irradiation. *Adv. Powder Technol.* **2018**, *10*, 2491–2500. [[CrossRef](#)]
50. Ma, Y.; Lu, N.; Lu, Y.; Guan, J.-N.; Qu, J.; Liu, H.-Y.; Cong, Q.; Yuan, X. Comparative study of carbon materials synthesized “greenly” for 2-CP removal. *Sci. Rep.* **2016**, *6*, 29167. [[CrossRef](#)]

Disclaimer/Publisher’s Note: The statements, opinions and data contained in all publications are solely those of the individual author(s) and contributor(s) and not of MDPI and/or the editor(s). MDPI and/or the editor(s) disclaim responsibility for any injury to people or property resulting from any ideas, methods, instructions or products referred to in the content.